

The Crab Nebula’s Moving Wisps in Radio

M. F. Bietenholz

Department of Physics and Astronomy, York University, North York, M3J 1P3, Ontario, Canada

D. A. Frail

National Radio Astronomy Observatory, Socorro, New Mexico, 87801, USA

J. J. Hester

Department of Physics and Astronomy, Arizona State University, Tempe, Arizona, 85287, USA

ABSTRACT

We present three high resolution radio images of the Crab nebula, taken in 1998.6, 1998.8 and 2000.1 with the VLA. These are the best radio images of the Crab to date. We show that, near the pulsar, there are significant changes between our three observing epochs. These changes have an elliptical geometry very similar to that of the optical wisps. One radio wisp in particular can be unambiguously identified between two of our observing epochs, and moves outward with an apparent velocity of $\sim 0.24c$. The similarity in both morphology and behavior of the present radio wisps to the optical wisps suggests that they are associated. This implies that the radio wisps, like the optical ones, are likely manifestations of the shock in the Crab pulsar’s wind. This suggests that the radio emitting electrons are accelerated in the same region as the ones responsible for the optical to X-ray emission, contrary to most current models.

Subject headings: ISM: Individual (Crab Nebula) — Radio Continuum: ISM — supernova remnants

1. Introduction

The Crab Nebula is one of the most important objects in astrophysics. It is a beautiful example of a pulsar powered nebula, and is also the most accessible pulsar nebula. Each generation of observations has revealed new intricacies to its structure. Recent results have highlighted the remarkable nature of the region surrounding the Crab Nebula’s pulsar, where the pulsar wind is injected into the nebula. A remarkable image of this region from the Chandra X-ray observatory (Weisskopf et al. 2000) shows a complex geometry consisting of a tilted toroidal structure with a jet along the symmetry axis of the torus. A recent sequence of images from the Hubble Space Telescope (HST) by Hester et al. (1996) revealed astonishing details in this region. In particular, there is a series of elliptical ripples in this region, which are usually called

“wisps”.

The wisp region has long been known to be rapidly variable (Lampland 1921; Scargle 1969), but only recently has the nature of the variability been conclusively established: Hester et al. (1996; see also Hester 1998) and Tanvir, Thomson, & Tsikarishvili (1997) have demonstrated that the wisps are variable on time-scales as short as a few days and that they are moving outwards with apparent speeds of up to $0.7c$. Early Chandra results indicate that the X-ray structure is also variable, on timescales of ~ 10 days.

At the center of the Crab Nebula, and of the wisp region, the rapidly spinning Crab pulsar is slowing down, and thus losing energy at the rate of 5×10^{38} erg s^{-1} . This bulk of this energy emerges from the pulsar as a highly collimated wind of relativistic particles and magnetic field. This outflow is randomized at a shock, where it comes into equi-

librium with its surroundings (Rees & Gunn 1974) and then flows into the body of the nebula, where it gives rise to the synchrotron emission we observe from the body of the nebula. However, the process by which this transfer of energy happens is not yet well understood (see e.g. Begelman 1999; Arons 1998; Hester 1998; Chedia et al. 1997).

Since almost all the pulsar’s spindown energy is accounted for in the body of the nebula, we know that the transfer of this energy is quite efficient. Only a very small fraction of the energy seems to be radiated directly from the region where the wind is randomized: the wisps are now thought to be associated with the shock which terminates the highly collimated outflow from the pulsar and randomizes it before it enters the body of the nebula. These features are our only observational window into the process by which the pulsar outflow is converted into the relativistic gas and magnetic field which fill the body of the nebula.

A feature with an arc-like geometry similar to that of the optical wisps was observed in the radio spectral index by Bietenholz & Kronberg (1992), who also observed changes in the radio emission from the center of the nebula over a period of five years. Our goal with these observations is to investigate the nature of the radio synchrotron emission from the wisp region, and to compare it to the synchrotron emission from the optical wisps. In particular, we will investigate whether the radio wisps are also rapidly variable, since the extant observations of them show only that they are variable on a 5 year timescale.

2. Observations and Data Reduction

We observed the Crab Nebula using the NRAO VLA¹ in the 5 GHz band. Table 1 shows details of our three observing runs, all of which were done using the VLA in the B configuration. Due to scheduling reasons, our observing run in February 2000 was split into two segments, which we combined, and we refer to this combined data set as our 11 February 2000 epoch. At each of these sessions, we observed at a spaced pair of frequencies (within the 5 GHz band) in order to increase our u - v coverage, since good u - v coverage is critical

¹The NRAO Very Large Array is a facility of the National Science Foundation operated under cooperative agreement by Associated Universities, Inc.

when imaging an object as extended as the Crab. In addition, we chose different pairs of frequencies for the 10 Feb. and the 12 Feb. 2000 observing runs, since these two runs had roughly the same range in hour angle.

Our primary goal was to investigate any rapid variations in the nebular structure. Since a speed of c represents a proper motion of only $\sim 3''$ per month, we do not expect the large scale structure of the nebula to change very much on short timescales. We do know that the radio synchrotron nebula is expanding at 0.13% year⁻¹ (Bietenholz et al. 1991). The effect of this expansion is both predictable, since the rate is known, and is also quite small over the timespan of our observations: the most rapid motion due to the overall expansion rate is $< 0''.3$ yr⁻¹.

The fact that the large scale structure of the nebula is not expected to change over our timespan is crucial to our strategy: an interferometer like the VLA measures the spatial Fourier transform of the sky brightness, and is sensitive only to a range of spatial frequencies determined by the length of the interferometer baselines and the observing frequency. For example, in the B configuration at 5 GHz, the VLA is sensitive only to structure on spatial scales between $\sim 1''.3$ and $\sim 50''$. The Crab Nebula, however, exhibits structure at spatial scales from $\sim 6'$ down to $< 1''$. Typically in such cases, one would obtain the larger scale structure from VLA observations in more compact array configurations. However, since VLA configuration changes occur only once every four months, that approach is not compatible with our goal of obtaining time-resolved observations.

Our solution to this problem is to use maximum entropy deconvolution (AIPS task VTESS; see Cornwell & Evans 1985, Cornwell 1988), which allows us to recover the large scale structure by supplying a low resolution support (default) in the deconvolution process. The deconvolved image is then biased to be as close to the support as is allowed by the data. We chose this support to be the same for all three of our epochs² which serves to make any differences between the epochs be only such as are demanded by the data.

As our support, we used an image of the Crab

²We did scale the support according to the known expansion of 0.13% year⁻¹ but the effect of this is minimal.

made using data taken in 1987, at 5 GHz, using the B, C and D configurations of the VLA (Bietenholz & Kronberg 1990; 1991). We convolved this image with a round Gaussian of full-width at half-maximum (FWHM) $20''$, and scaled it to account for the general expansion of the radio nebula since 1987. Because we have only B array data at the current epochs of interest, the structure in our images on the largest spatial scales, i.e. those $> 1'$, is derived predominately from the support image, and we thus have very little information on any changes that might occur at these spatial scales. As we have argued above, however, there is little reason to expect rapid variations on these scales. On spatial scales smaller than $\sim 30''$ on the other hand, our u - v coverage is excellent, and we believe that our images reliably indicate the structure of the nebula, and in particular, changes therein from one epoch to another.

3. Results

An image of the Crab Nebula on 11 February 2000 is shown in Figure 1. The restoring beam size was $1''.4$ (this restoring beam size was conservatively chosen as a common size for all three epochs). The background rms level was $76 \mu\text{Jy beam}^{-1}$ before applying the primary beam correction, and the peak flux was $46.6 \text{ mJy beam}^{-1}$. This is the highest dynamic range and resolution radio image yet produced of the Crab Nebula. We note that it is superior to the three and four-configuration VLA images of Bietenholz & Kronberg (1990; 1991) — on which it is partly based through the use of those images as a support — because of our presently increased u - v coverage at the higher spatial frequencies.

The images taken 1998 August and October were very similar, and so we do not reproduce them in their entirety. They had background rms levels of 100 and $82 \mu\text{Jy beam}^{-1}$ respectively. Instead, we present a *difference* image: Figure 2 shows the difference between the images of October and August 1998.

On this difference image a prominent series of elliptical ripples are visible near the center of the nebula. The brightness of these ripples is several times that of the background noise level. Such ripples are only visible near the pulsar position: Figure 2 shows that, in the rest of the nebula,

any difference features are of lower amplitude and larger spatial scale, and likely due to noise, missing short-spacings, and errors in the deconvolution. The elliptical ripples show a remarkable similarity in geometry with the elliptical wisps seen in the optical (Hester et al. 1995; Hester et al. 1996) and the torus visible in the X-ray (Aschenbach & Brinkman 1975; Weisskopf et al. 2000). Figure 3 shows a region near the pulsar of the radio difference image between 1998 October and 2000 February, and a corresponding difference image between two HST images taken 1.5 months apart and convolved to the same resolution (note that the images in this figure have been rotated by -47°). In particular, the implied inclination angle (assuming that the features are intrinsically circular) is similar to that in both the optical and the X-ray. If the ripples were an artefact, such a coincidence in geometry with the real features observed at other wavelengths would be quite unlikely. While moving features seem to exist over roughly the same region in both the optical and radio images, the largest features in the radio are further from the pulsar than the largest optical features are.

In order to make the motions from one epoch to the next better visible in reproductions, we show in Figure 4 high-pass filtered views of the center of each of our three images. We used a Gaussian high-pass filter with a FWHM of $25''$, which serves to accentuate the relatively faint wisp-like mobile features. We will call the most mobile feature wisp *a*, and we indicate its position in 1998 August by a black line on all three images in order to show the displacement in the subsequent epochs.

These motions are real: they occur on spatial scales of a few arc-seconds, exactly those to which we are sensitive and for which we have excellent u - v coverage. In order to further ascertain that these motions were not some form of artefact due to the deconvolution process, we performed several tests. Firstly, we deconvolved the 1998 August image using the October image as a support, instead of our usual low-resolution image. This further biases the images to be as similar as is allowed by the data. The ripples remained essentially unchanged. Secondly, expanding or contracting the default image by 2% also left the ripples unchanged, but resulted in a poorer image. Lastly, we self-calibrated the 1998 August u - v data both in amplitude and

TABLE 1
OBSERVING RUN DETAILS

Date	Length (hrs)	Frequencies (MHz)	Midpoint (days since 1998.0)
1998 Aug 9	9.6	4615, 4885	221.7
1998 Oct 13	10.1	4615, 4885	286.5
2000 Feb 10	3.7	4749, 4996	772.1
2000 Feb 12	5.7	4615, 4885	774.0
(combined Feb 2000)	9.4	4615, 4749, 4885, 4996	773.1 ^a

^aThe midpoint for the combined February 2000 runs was taken to be the weighted mean of the midpoints of the two individual days.

phase, using the October image as a model, and vice versa, and then re-imaged. Again, the ripples are essentially unchanged, implying that they cannot be ascribed to any calibration anomalies.

Finally, in order measure the speeds of features, we plotted profiles through the high-pass filtered images. Figure 5 shows profiles for our three epochs, drawn through the pulsar at position angles, p.a., of -11° , chosen to pass through the most mobile wisp, and at -90° , chosen so as to pass through a mobile feature on the opposite side of the pulsar. There are numerous changes in addition to the motion of wisp *a* indicated in Fig. 4 above. However, with our very coarse sampling in time, the identification of features from one epoch to the next is difficult. We note that the pulsar, which is known to be quite variable but has a mean flux density of 1.4 mJy at 4.8 GHz (Lorimer et al. 1995), is visible as a variable peak at the origin in the profiles.

The identification is wisp *a* between 1998 August and October is unambiguous. It moves with an apparent velocity of $0.24 \pm 0.06c$. We indicate this motion with a solid line on Fig. 5*a*. By 2000 February 11, the identification is no longer completely unambiguous — we mark the motion derived from the likeliest identification in Fig. 5*a* with a dashed line. This identification implies an average apparent speed between 1998 August and 2000 February of $0.28 \pm 0.01c$, which is consistent with the speed between 1998 August and October. On the opposite side of the pulsar, the

most prominent moving feature is seen on the profile at p.a. = -90° . We call this feature the counter-wisp, and mark its motion in Fig. 5*b*. The speed between 2000 August and October is not reliably determinable, but the apparent speed between 1998 (taking the average of August and October) and 2000 February is $0.08 \pm 0.02c$, and this motion marked in Fig. 5*b*. We note that because of the large time interval and the complexity of the changes between our 1998 and 2000 epochs, the identification of features over this time-span is necessarily somewhat more tentative.

Assuming an inclination angle of 30° , we can calculate the true speed of the features above: wisp *a* has a true speed of $0.38 \pm 0.01c$, (assuming that the above identification in Feb. 2000 is correct; see Fig. 5*a*). The counter-wisp has a true speed of $0.19 \pm 0.05c$.

4. Discussion

We have shown that there are rapidly moving features, with velocities $\lesssim c/3$, visible in the radio emission from the Crab Nebula. These features have an arc-like geometry similar to that of the optical wisps. Bietenholz & Kronberg (1992) had already reported the existence of similarly shaped features near the center of the nebula, apparent in the radio spectral index. They noted the possibility that these features might in fact be temporal changes rather than true spectral index features, because the two images from which they derived the spectral index were effectively taken several

months apart³. In light of the present results it seems likely that the features reported in Bietenholz & Kronberg (1992) were in fact the result of temporal changes, rather than true spectral index anomalies. We cannot of course exclude the presence of true spectral index variations, but the data so far at hand do not demand them.

We propose that these rapidly variable radio wisps are associated with the similar features seen in the optical and the torus visible in the X-ray. The precise geometry of the radio features is harder to discern than that of the optical wisps due to the presence of a relatively much brighter complex background provided by the rest of the nebula. Nonetheless our difference images give a distinct picture of the temporal changes in these features, and clearly show an elliptical geometry. In fact, the ellipticity is the same as that of both the optical wisps and the X-ray torus, suggesting that, like the optical wisps and the X-ray torus, the radio wisps are circular features seen at the same inclination angle of $\sim 30^\circ$.

Like the optical wisps, the radio wisps seem to be moving outward (although this is not clearly established by our observations, since we have only three epochs and sub-optimal time sampling, the unambiguously identified wisp *a* is moving outwards between August and October 1998). Furthermore, we measure speeds of $\lesssim c/3$ for the features which we can identify from one epoch to the next. This is in fact the expected speed for the post-shock flow (Blandford & Rees 1974) and consistent with the speeds measured in the optical (Hester et al. 1996; Hester 1998; Tanvir et al. 1997) and inferred from the X-ray (Pelling et al. 1987). These arguments strongly suggest that the presently observed radio wisps are associated with the optical wisps and the X-ray torus.

In order to discuss the implications of these observations, we will briefly describe our theoretical understanding of the Crab Nebula. As mentioned in § 1, the visible synchrotron nebula is powered by the spindown energy of pulsar. This energy emerges from the pulsar in the form of a collimated, highly relativistic wind, which con-

sists of some combination of particles and magnetic field. The coupling to the outer boundary condition, namely the outside of the observable synchrotron nebula which moves with $v \ll c$, requires a shock in the wind. It is at this shock that the particle velocities are randomized, and it is the post-shock wind which then supplies the relativistic particles and the magnetic field responsible for the nebular synchrotron emission. The wisps are thought to be manifestations of this termination shock, since pressure balance arguments place the location of the shock roughly at the wisp location (Rees & Gunn 1974). Similar features have been seen near other pulsars (Bietenholz, Frail, & Hankins 1991; Frail & Moffett 1993), and so they may be a common manifestation of the interaction of a pulsar wind with its surroundings. In particular, the wisps are thought to be associated with the shock in the equatorial sector of the pulsar wind, since both the optical and especially the X-ray observations (Weisskopf et al. 2000) clearly show a toroidal geometry. (We note that polar features are also seen in both the optical and the X-ray, but as yet we cannot conclusively identify any polar features in the radio).

The precise mechanism of wisp formation, however, is not yet well understood (Bietenholz & Kronberg 1992; Chedia et al. 1997; Hester 1998; Arons 1998; Begelman 1999). Also, while the radio spectral index is very uniform over the nebula (Bietenholz et al. 1997), suggesting a single and presumably central source for all the radio emitting electrons, their origin in the shock near the pulsar is not yet understood (see e.g., Atoyan 1999; Arons 1998). At the termination shock of the wind, one expects that the mean Lorentz factor, γ , of the post-shock particles to be roughly equal to that in the wind, which is widely thought to be $\sim 10^6$ (Rees & Gunn 1974; Kennel & Coroniti 1984; Melatos & Melrose 1996; Arons, 1998). However, this would produce essentially no radio-emitting, i.e. $\gamma \sim 10^3$ electrons.

For example, the model of Arons (1998; see also Gallant & Arons 1994) can account for wisps and also the observed nebular spectrum from the optical to the X-ray, but it cannot account for the radio-emitting electrons. Arons suggests that a slower, high-latitude wind might produce the radio emitting electrons. In the model of Atoyan (1999), which can account for the entire nebular

³The spectral index was between 5 GHz and 1.4 GHz. The 5 GHz B-array data were taken on 1987 November 25, while the resolution-matched 1.4 GHz A-array data were taken on 1987 July 7.

spectrum, the radio emitting electrons are of historical origin, having been emitted when the pulsar was younger and spinning much more rapidly. However, in neither of these cases would radio-emitting electrons be accelerated in the current wisp region. Thus the detection of wisps in the radio implies that the acceleration of particles in the equatorial shock termination region produces low energy radio-emitting electrons as well as those at higher energies responsible for the optical and higher synchrotron emission.

In summary, we present new radio images of the Crab Nebula, with higher resolution and dynamic range than those previously available. We show that there are significant changes occurring over periods of two months and one year. An arc-like feature, or wisp, is seen to be moving outwards, and images of the *differences* between successive pairs of our three observing epochs clearly show numerous features which have an elliptical geometry. We propose that these radio wisps are associated with the optical wisps, which suggests that acceleration mechanism producing radio-emitting electrons is the same as, or at least co-spatial to, that producing the more energetic electrons responsible for the nebular optical and X-ray synchrotron emission. Future, more highly time-resolved observations will hopefully allow us to establish the exact nature and speed of the motions.

Research at York University was partly supported by NSERC. We thank Barry Clark for his patience with the scheduling difficulties involved in these observations.

REFERENCES

- Arons, J. 1998, in *The Relationship Between Neutron Stars and Supernova Remnants*, eds. R. Bandiera et al., (*Memorie della Società Astronomica Italiana*, vol. 69, no. 4), 989
- Aschenbach, B., & Brinkmann, W. 1975, *A&A*, 41, 147
- Atoyan, A. M. 1999, *A&A*, 346, L49
- Begelman, M. C. 1999, *ApJ*, 512, 755
- Bietenholz, M. F., Frail, D. A., & Hankins, T. H. 1991, *ApJ*, 376, L41
- Bietenholz, M. F., & Kronberg, P. P. 1990, *ApJ*, 357, L13
- Bietenholz, M. F., & Kronberg, P. P. 1991, *ApJ*, 368, 231
- Bietenholz, M. F., & Kronberg, P. P. 1992, *ApJ*, 393, 206
- Bietenholz, M. F., Kronberg, P. P., Hogg, D. E., & Wilson, A. S. 1991, *ApJ*, 373, L59
- Bietenholz, M. F., Kassim, N., Frail, D. A., Perley, R. A., Erickson, W. C., Hajian, A. R. 1997, *ApJ*, 490, 291
- Blandford, R. D., & Rees, M. J. 1974, *MNRAS*, 169, 395
- Chedia, O., Lominadze, J., Machabeli, G., McHedlishvili, G., & Shapakidze, D. 1997, *ApJ*, 479, 313
- Cornwell, T. J. 1988, *A&A*, 202, 316
- Cornwell, T. J., & Evans, K. F., 1985, *A&A*, 143, 77
- Frail, D. A., & Moffett, D. A. 1993, *ApJ*, 408, 637
- Gallant Y. A., & Arons, J. 1994, *ApJ*, 435, 230
- Hester, J. J., et al. 1995, *ApJ*, 448, 240
- Hester, J. J., Scowen, P. A., Sankrit, R., Michel, F. C., Graham, J. R., Watson, A., & Gallagher, J. S. 1996, *BAAS*, 188, 7502 (see also <http://www.stsci.edu/pubinfo/PR/96/22.html>)
- Hester, J. J. 1998, in *The Relationship Between Neutron Stars and Supernova Remnants*, eds. R. Bandiera et al., (*Memorie della Società Astronomica Italiana*, vol. 69, no. 4), 883
- Kennel C. F., & Coroniti, F. V. 1984, *ApJ*, 283, 694
- Lampland, C. O. 1921, *PASP*, 33, 79
- Lorimer, D. R., Yates, J. A., Lyne, A. G., & Gould, D. M. 1995, *MNRAS*, 273, 411
- Melatos, A., & Melrose, D. B. 1996, *MNRAS*, 279, 1168
- Pelling, R. M., Paciesas, W. S., Peterson, L. E., Makishima, K., Oda, M., Ogawara, Y., & Miyamoto, S. 1987, *ApJ*, 319, 416
- Rees, M. J., & Gunn, J. E. 1974, *MNRAS*, 167, 1
- Scargle, J. D. 1969, *ApJ*, 156, 401
- Tanvir, N. R., Thomson, R. C., & Tsikarishvili, E. G. 1997, *New Astronomy*, 1, 311
- Weisskopf, M. C., et al. 2000, *ApJ*, 536, L81

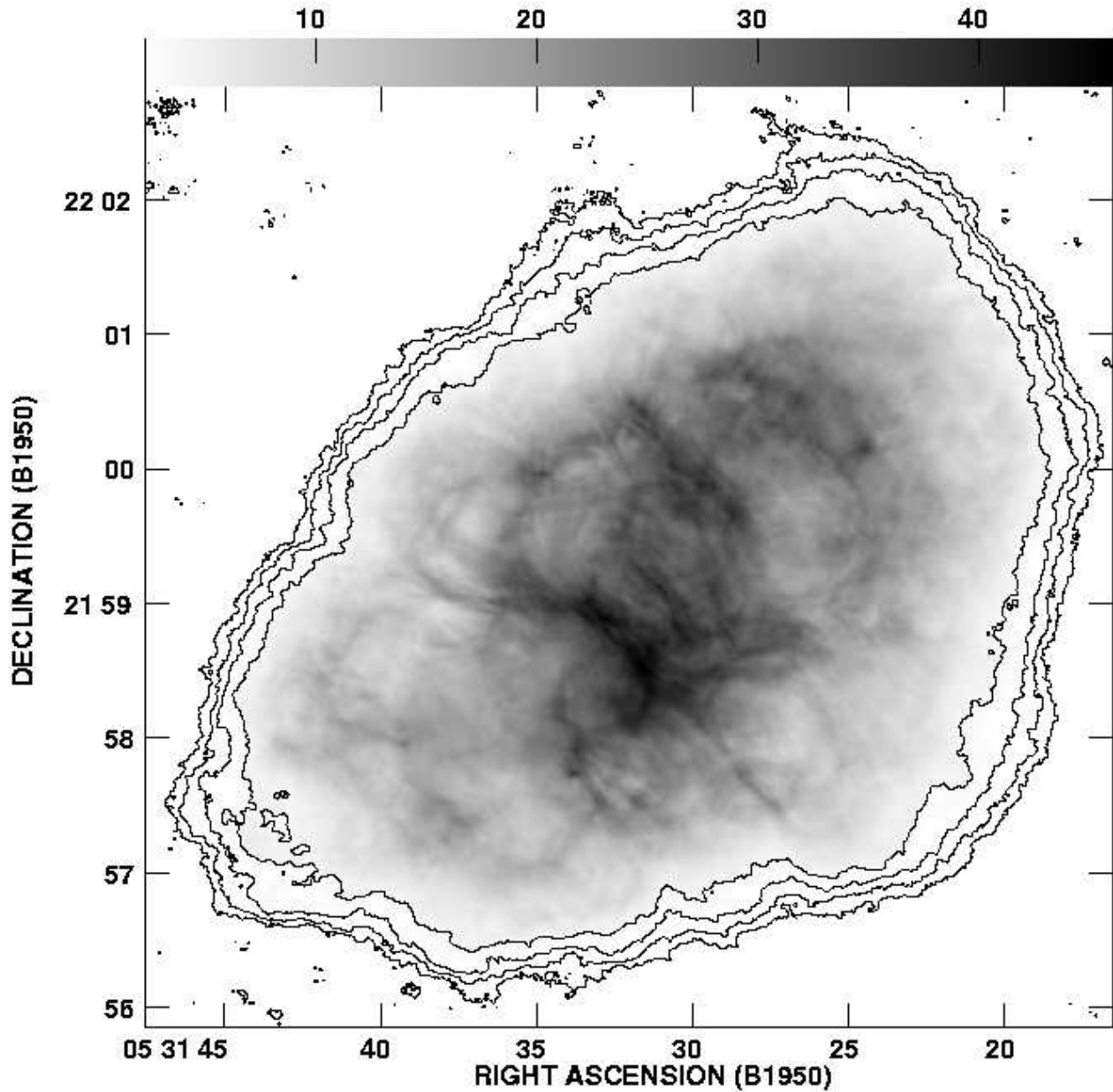


Fig. 1.— The image of the Crab at 5 GHz on 2000 February 11 (from data taken on Feb. 10 and 12), after primary beam correction. The FWHM size of the restoring beam was $1''.4$. The peak flux density is $46.6 \text{ mJy beam}^{-1}$, and the exterior rms was $76 \mu\text{Jy beam}^{-1}$ before primary beam correction. The contours are drawn at 0.75, 2, 4 and 8% of the peak, and the greyscale is in mJy beam^{-1} . Maximum entropy deconvolution was used with a support to recover the low spatial frequency structure (see text, § 2) for details).

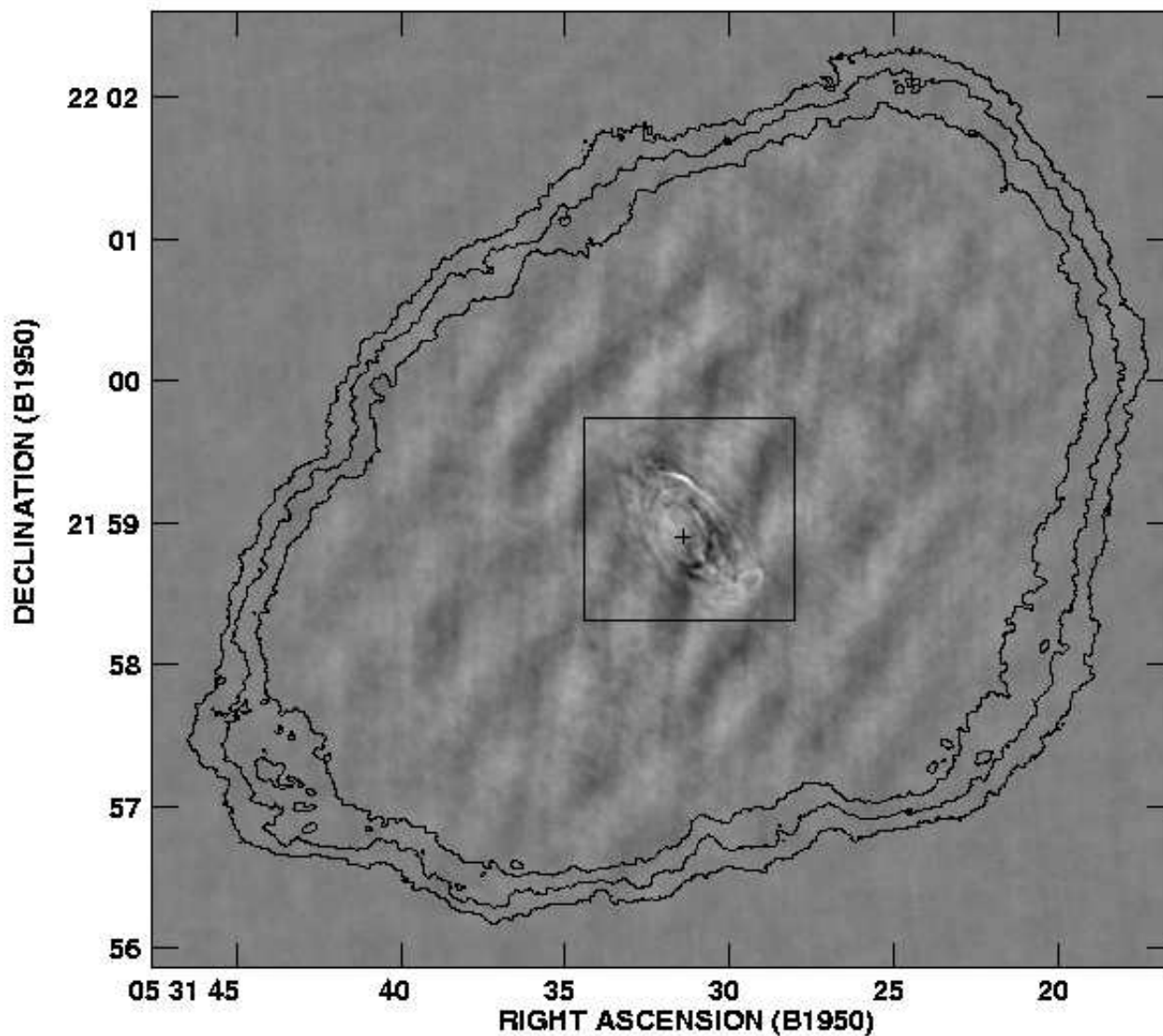


Fig. 2.— The differences between our 1998 October 13 and 1998 August 9 images in greyscale, with the greyscale ranging from +5 to -5 mJy beam^{-1} . The FWHM size of the restoring beam was $1''.4$. For reference, we also show the the 2, 5, and 10% contours from the 2000 February 11 image, and indicate the pulsar position by a cross. The box indicates the region of the high-pass filtered images shown below in Fig. 4

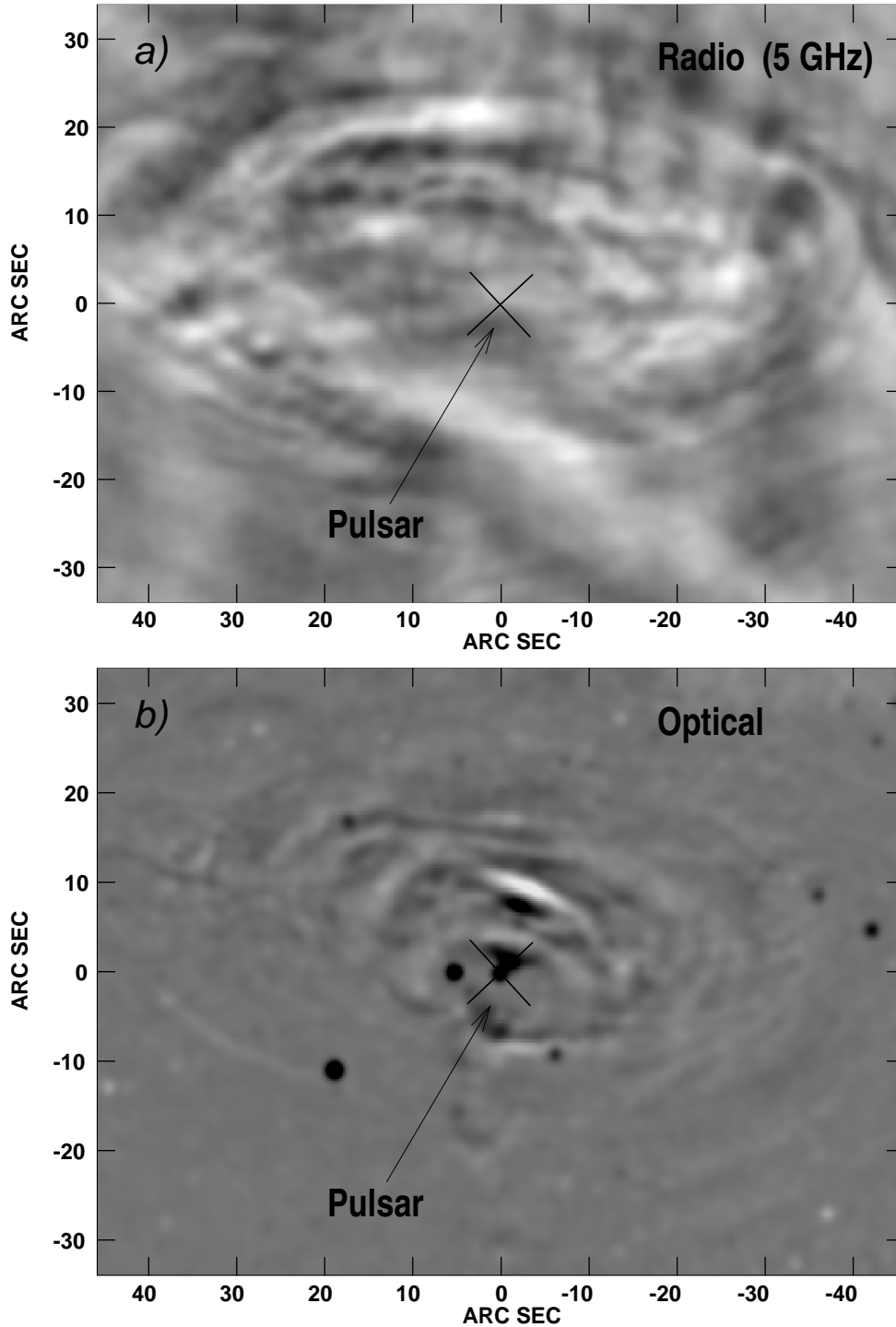


Fig. 3.— The difference features in the optical and radio. The images have been rotated by -47° . The cross is drawn in the N-S E-W direction, and shows location of the pulsar. In *a*) we show the radio difference image between 2000 February 11 and 1998 October 13 (the greyscale ranges from $+5$ to -5 mJy beam $^{-1}$, and the convolving beam size was $1''.4$ FWHM). In *b*) we show the difference between the HST images from 2000 October 23 and September 9, convolved also to $1''.4$ FWHM resolution.

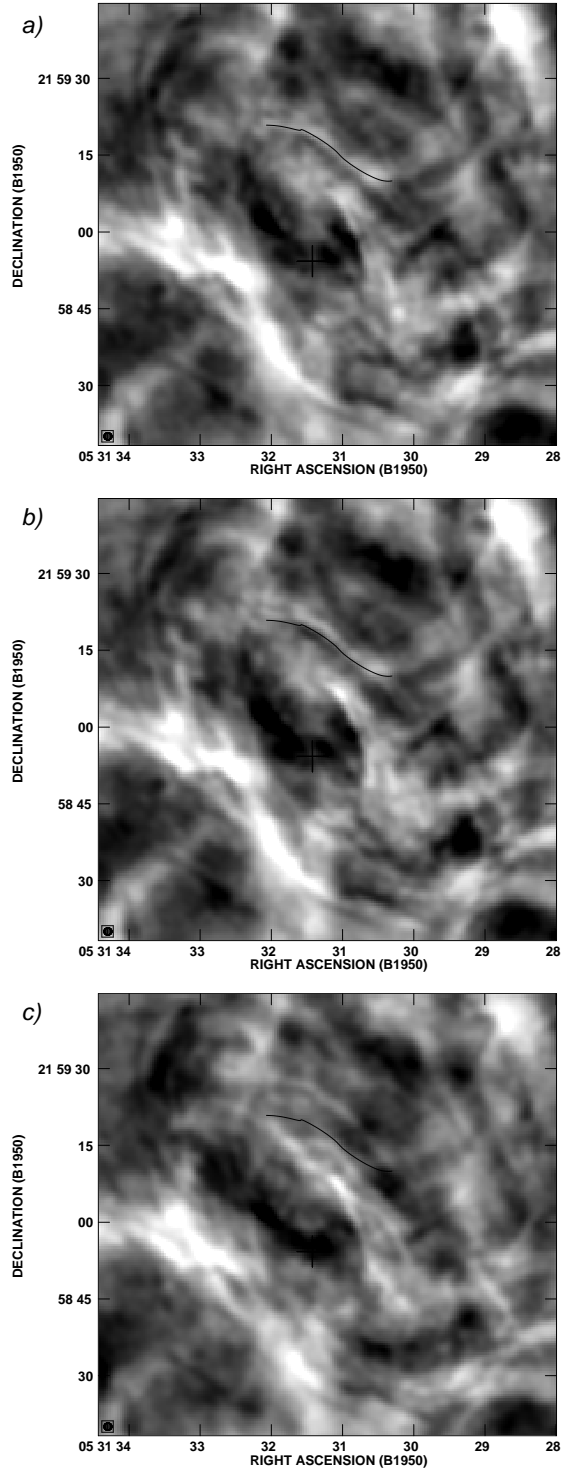


Fig. 4.— High-pass filtered images of the region near the pulsar, showing the mobile wisps. The images have been high-pass filtered with a Gaussian of FWHM $25''$. The restoring beam again has a FWHM size of $1''.4$, shown at lower left. The position of wisp *a* on 1998 August 9 is indicated on all three images to show its displacement. In *a*) we show the image from 1998 August 9, in *b*) that from 1998 October 13, and in *c*), that from 2000 February 11.

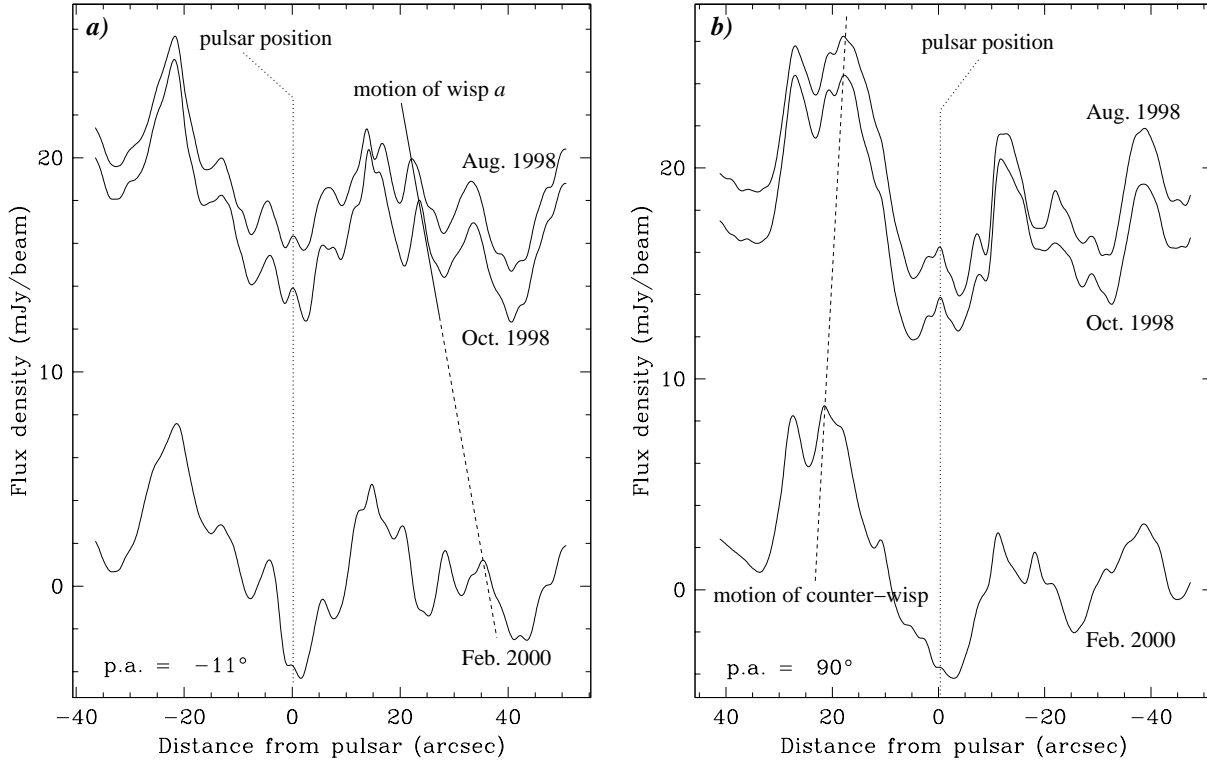


Fig. 5.— Profiles through the center of the Crab at three epochs. The profiles were made from the high-pass filtered images shown in Fig. 4. In each case the bottom profile is that from 2000 February 11. The middle and the upper profiles are those from 1998 October 13 and August 9, respectively, and have been artificially shifted upwards by an amount proportional to the time difference to the 2000 February epoch. The profiles are drawn through the pulsar position ($5^{\text{h}} 31^{\text{m}} 31^{\text{s}}.423$, $21^{\circ} 58' 54''.26$), which is indicated by the dotted vertical line. In *a*) we show profiles drawn at a p.a. of -11° , with a +ive displacement being to the NW. The motion of wisp *a* is indicated, with the solid line indicating the secure identification of this feature between 1998 August and October, and the dashed line showing the likeliest identification in 2000 February. In *b*) we show profiles in R.A. or at a p.a. of 90° . The motion of the counter-wisp is indicated.